Choice of no-slip curved boundary condition for lattice Boltzmann simulations of high-Reynolds-number flows

Sathish K. P. Sanjeevi, Ahad Zarghami, and Johan T. Padding[*]

Process and Energy Department, Delft University of Technology, Leeghwaterstraat 39, 2628 CB Delft, The Netherlands

Various curved no-slip boundary conditions available in literature improve the accuracy of lattice Boltzmann simulations compared to the traditional staircase approximation of curved geometries. Usually, the required unknown distribution functions emerging from the solid nodes are computed based on the known distribution functions using interpolation or extrapolation schemes. On using such curved boundary schemes, there will be mass loss or gain at each time step during the simulations, especially apparent at high Reynolds numbers, which is called mass leakage. Such an issue becomes severe in periodic flows, where the mass leakage accumulation would affect the computed flow fields over time. In this paper, we examine mass leakage of the most well-known curved boundary treatments for high-Reynolds-number flows. Apart from the existing schemes, we also test different forced mass conservation schemes and a constant density scheme. The capability of each scheme is investigated and, finally, recommendations for choosing a proper boundary condition scheme are given for stable and accurate simulations.

I. INTRODUCTION

In the last two decades, there has been growing interest in using the lattice Boltzmann method (LBM) as a promising alternative technique for simulating various fluid flow problems [1–5]. Unlike the conventional computational fluid dynamics (CFD) methods, the LBM does not solve the incompressible Navier-Stokes equations directly, but instead the fluid flow is described in terms of a discrete kinetic equation based on the particle distribution functions [6]. The standard LBM consists of two steps, namely, collision and streaming. The collision step describes the local changes of particle density due to collisions at each grid node. In the streaming step, distribution functions are streamed from lattice nodes to their neighbors. Macroscopic quantities, such as density or velocity, are recovered as statistical moments of the particle distribution functions. Therefore, the particle distribution functions are the essential objects of the method.

Since the LBM is performed on equidistant Cartesian grids, boundary condition schemes were first introduced for straight walls. The bounce-back (BB) scheme is the most common, simplest, and exactly mass conserving scheme for the solid wall boundary condition and provides a particularly straightforward approach for modeling no-slip conditions on solid walls. In this scheme, when a particle distribution streams to a wall node, it reflects back to the fluid node along its incoming link [6,7]. The onsite BB and the mid-grid BB are two types of BB schemes [8]. In the onsite BB scheme, the physical boundary nodes lay exactly at the lattice nodes. In the mid-grid BB scheme, the solid boundary is located exactly mid-plane between the boundary fluid node and the off-lattice node inside the solid. The onsite BB scheme is first-order accurate, whereas the mid-grid BB scheme provides second-order accuracy in both

space and time [6]. Alternative wall boundary conditions with second-order accuracy were proposed by various researchers [8–11]. For all of these boundary condition treatments, the solid wall should be aligned with the computational grid [12,13].

The above-mentioned schemes have been quite successful in improving numerical accuracy for flows with flat-wall boundaries aligned with the computational grid. However, they fail to accurately simulate curved boundaries (or flat-wall boundaries inclined with respect to the computational grid). For simulating flow with curved boundaries, we need to determine the distribution functions at the nodes nearest the curved boundaries based on the known boundary conditions. The use of BB schemes with curved boundaries leads to staircase shaped boundaries [14,15]. It should be noted that with a stair-shaped approximation, not only the fidelity of real geometry is lost, it may also introduce undesired errors (such as a nonzero wall velocity) in a simulation that could contaminate the results [16].

In the literature, various boundary treatments have been developed that provide a more accurate treatment of curved boundaries to determine the distribution functions on the boundary nodes. The first method for treating curved boundaries with the LBM was proposed by Filippova and Hanel based on interpolation or extrapolation of the distribution functions [17]. It relies on ghost cells inside solid walls and applies a linear interpolation of particle distributions to enforce the boundary condition at the exact boundary location. This scheme has second-order accuracy. However, it suffers from poor numerical stability, particularly when the near-wall fluid node is very close to the solid boundary. The stability issue of this scheme was improved by Mei *et al.* [18] by placing the boundary node used for velocity interpolation to the closest fluid nodes, if the actual wall boundary is too close to a solid node. The stability of this method was further improved by various researchers [19–21].

─────────
[*]J.T.Padding@tudelft.nl

Bouzidi *et al.* [22] proposed a method with second-order accuracy that does not require the extrapolations from the ghost nodes in solid wall. The proposed scheme combines the bounce-back concept with linear or quadratic interpolation of the distribution functions from the internal fluid nodes. The accuracy of this method has been improved by Ginzburg and d'Humières [23] and extended to moving boundaries by Lallemand and Luo [24]. Yu *et al.* [25] proposed a unified version of the Bouzidi scheme by using a two-step sequential interpolations to avoid the discontinuity in the boundary treatment. Yin and Zhang [26] modified the Ladd scheme with the boundary velocity at the mid-grid computed using interpolation or extrapolation between the boundary node and fluid node. In addition to the above-mentioned boundary methods, several other approaches have been developed for simulating curved boundaries in the LBM [27–30]. The different boundary conditions of LBM are compared on different lattice configurations by Nash *et al.* [31].

Usually when using the interpolation- or extrapolation-based curved boundary schemes in the LBM simulations, the mass of the system is not conserved exactly. In other words, there will be mass loss or gain at each time step during the simulation, which is called mass leakage in the literature. Lallemand and Luo [24] showed that the use of interpolation breaks mass conservation near curved boundaries. They found that the inaccuracy in evaluating momentum transfer can lead to a net mass flux at the boundary. There are also flux based finite-volume boundary schemes that are designed to conserve mass [32,33]. However, these require estimates of the cut-cell volume of the boundary cells, which add further complexity. From an implementation point of view, link based interpolation methods are much simpler. Various mass conserving boundary treatments have been proposed to avoid the mass leakage issue and improve the numerical stability of the simulations [34–36]. However, such proposed mass conserving boundary conditions either still exhibit minor leakage [34], are not analyzed rigorously for mass leakage through various test cases [32,35], or are applicable only for specific problems such as tangential boundaries [36]. In general, such a mass leakage does not affect simulation results for inflow-outflow boundaries [37]. However, the mass leakage accumulates over time for a periodic flow, driven by gravity. Such a flow problem is widely used in different areas such as flows around stationary arrays of particles and flows through porous media. For low Re flows, such a leakage is minor and can be ignored in general. However, at high Re, the change in system mass is large and cannot be ignored. The issue becomes even severe in the case of unsteady periodic flows, where a large number of time steps is required to reach statistical equilibrium. This subsequently results in drift in system mass and, therefore, constantly increasing or decreasing forces.

Our objective is to keep the grid Re high (relatively coarser grid and lower viscosity) since the mass leakage effects are directly a consequence and proportional to the grid Re than the flow Re itself. By this, we imply the importance of achieving good solution accuracy using a coarse grid against finer grid simulations as they are computationally more expensive.

Up to this point, there has not yet been a systematic comparison of the performance of curved boundary schemes with focus on mass leakage. We test the accuracy of most popular curved boundary condition schemes and schemes that showed potential for solving the mass leakage issue. It is the aim of this paper to provide such a comparison for cases with significant mass leakage issue, with focus on high Re flows. Further, in this paper we introduce forced conservation schemes that enforce strict mass conservation and test their performance.

The rest of this paper is organized as follows. We briefly introduce the LBM scheme in Sec. II. The selected curved boundary condition schemes are briefly presented in Sec. III. Results and discussion are presented in Sec. IV followed by our recommendations and conclusions in Secs. V and VI, respectively.

II. LATTICE BOLTZMANN METHOD

The general lattice Boltzmann equation with the single-relaxation-time (SRT) approximation is written as [6]

$$f_\alpha(\boldsymbol{r} + \boldsymbol{e}_\alpha \Delta t, t + \Delta t) - f_\alpha(\boldsymbol{r}, t)$$
$$= -\frac{1}{\tau}\big[f_\alpha(\boldsymbol{r}, t) - f_\alpha^{\mathrm{eq}}(\boldsymbol{r}, t)\big] + S_\alpha, \qquad (1)$$

where f_α is the particle distribution function signifying the probability to find a particle at location $\boldsymbol{r}$ with a velocity in the direction α, f_α^{eq} is the equilibrium distribution, $\Delta t = 1$ is the time interval, $\tau = 1/\omega$ is the relaxation time, ω is the relaxation factor, and S_α represents a general body force in the direction α added to the equation. The equilibrium density distribution function is given by

$$f_\alpha^{\mathrm{eq}} = w_\alpha \rho \left[1 + \frac{(\boldsymbol{e}_\alpha \cdot \boldsymbol{u})}{c_s^2} + \frac{(\boldsymbol{e}_\alpha \cdot \boldsymbol{u})^2}{2c_s^4} - \frac{(\boldsymbol{u} \cdot \boldsymbol{u})}{2c_s^2}\right], \quad (2)$$

where $c_s = 1/\sqrt{3}$ is the lattice speed of sound and $\rho = \sum_\alpha f_\alpha$ and $\rho \boldsymbol{u}_\alpha = \sum_\alpha f_\alpha \boldsymbol{e}_\alpha$ are the local density and momentum, respectively. The lattice weights w_α and the discrete velocities $\boldsymbol{e}_\alpha$ of a D2Q9-lattice model are given by $w_{\alpha=0} = 4/9$, $\boldsymbol{e}_\alpha = (0,0)$, $w_{\alpha=1\sim4} = 1/9$, $\boldsymbol{e}_\alpha = (\cos\theta_\alpha, \sin\theta_\alpha)$ with $\theta_\alpha = (\alpha - 1)\pi/2$ and $w_{\alpha=5\sim8} = 1/36$, $\boldsymbol{e}_\alpha = \sqrt{2}(\cos\theta_\alpha, \sin\theta_\alpha)$ with $\theta_\alpha = (\alpha - 5)\pi/2 + \pi/4$. The viscosity and the pressure are calculated as $\nu = c_s^2(\tau - 0.5)$ and $p = \rho c_s^2$, respectively. It is clear that positivity of viscosity requires that $\tau > 0.5$. The standard LBM time step is performed in two steps, with the collision and the streaming steps as

$$\tilde{f}_\alpha(\boldsymbol{r}, t) = f_\alpha(\boldsymbol{r}, t) - \frac{1}{\tau}\big[f_\alpha(\boldsymbol{r}, t) - f_\alpha^{\mathrm{eq}}(\boldsymbol{r}, t)\big] + S_\alpha, \quad (3)$$

$$f_\alpha(\boldsymbol{r} + \boldsymbol{e}_\alpha \Delta t, t + \Delta t) = \tilde{f}_\alpha(\boldsymbol{r}, t), \qquad (4)$$

where $\tilde{f}_\alpha$ is the post-collision state of the distribution function but before the streaming. The effect of gravity as a body force [38] is applied as $S_\alpha = -3w_\alpha \rho(\boldsymbol{g} \cdot \boldsymbol{e}_\alpha)$, where $\boldsymbol{g}$ is the gravitational vector. For computing the fluid force on a body, the momentum exchange approach [14] after the streaming step is applied:

$$\boldsymbol{F} = \sum_{\mathrm{all}\,\boldsymbol{r}_b} \sum_{\alpha=1}^{8} \boldsymbol{e}_\alpha [f_\alpha(\boldsymbol{r}_b, t) + f_{\bar{\alpha}}(\boldsymbol{r}_f, t)], \qquad (5)$$
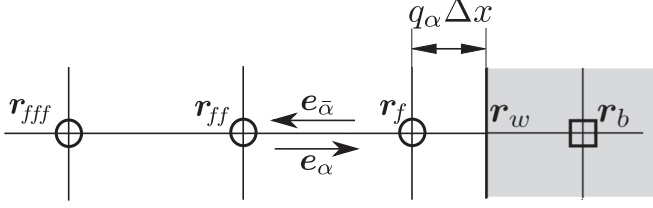
FIG. 1. One-dimensional representation of a regular lattice and a curved-wall boundary.

where $\bar{\alpha}$ denotes negative α direction and the summation is done over all boundary nodes $\boldsymbol{r}_b$, which are connected to a fluid node in the α direction according to $\boldsymbol{r}_b = \boldsymbol{r}_f + \boldsymbol{e}_\alpha \Delta t$.

III. TREATMENTS FOR CURVED-WALL BOUNDARY

Because a no-slip boundary with a wall can be modeled for each velocity direction separately, it is sufficient to consider a single lattice direction with a (curved) wall boundary surface at $\boldsymbol{r}_w$, as shown in Fig. 1. The curved-wall boundary may be located at an arbitrary position between the solid and fluid nodes (i.e., $\boldsymbol{r}_b$ and $\boldsymbol{r}_f$). The fraction of an intersected link in the fluid region is expressed using a parameter q as

$$q = \frac{|\boldsymbol{r}_w - \boldsymbol{r}_f|}{|\boldsymbol{r}_b - \boldsymbol{r}_f|}. \tag{6}$$

Various treatments for curved-wall boundary condition have been proposed in the literature to improve the accuracy of the LBM simulations. The work of Filippova and Hänel [17] and Mei *et al.* [18] were the first attempts to represent curved boundaries of a solid body. However, they are not stable for all relaxation times [34,39] and therefore are not considered in this work. Since the boundary schemes are formulated based on one-dimensional (1D) approximation of the lattice direction, two-dimensional (2D) test cases are sufficient to investigate their performance. For this reason, historically all or most of the proposed curved boundary condition literatures contain 2D test cases. However, their extensions to 3D are always straightforward and consistent. Therefore, we can also say that the results from here can be applicable for three dimensions (3D) in a straightforward manner. In this section, we briefly introduce the schemes that are analyzed in this work.

A. Mid-grid bounce-back scheme (MGBB)

The most widely used boundary condition for the LBM is the mid-grid bounce-back scheme. For a mid-grid bounce-back scheme, the solid boundary is assumed exactly halfway between the fluid node and the solid node (i.e., $q = \frac{1}{2}$). The mid-grid bounce-back scheme (see Fig. 1) is of second order and is given by

$$f_{\bar{\alpha}}(\boldsymbol{r}_f, t + \Delta t) = \tilde{f}_\alpha(\boldsymbol{r}_f, t). \tag{7}$$

B. Bouzidi schemes (L-Bouzidi and Q-Bouzidi) [22,24]

In this scheme, an interpolation is applied to calculate the unknown distribution function based on the position of the wall boundary. When linear interpolation is applied, the Bouzidi model (L-Bouzidi) is written as follows:

For $q < 0.5$,

$$f_{\bar{\alpha}}(\boldsymbol{r}_f, t + \Delta t) = (1 - 2q)\tilde{f}_\alpha(\boldsymbol{r}_{ff}, t) + 2q\,\tilde{f}_\alpha(\boldsymbol{r}_f, t), \tag{8}$$

and for $q \geqslant 0.5$,

$$f_{\bar{\alpha}}(\boldsymbol{r}_f, t + \Delta t) = \left(1 - \frac{1}{2q}\right)\tilde{f}_{\bar{\alpha}}(\boldsymbol{r}_f, t) + \frac{1}{2q}\tilde{f}_\alpha(\boldsymbol{r}_f, t). \tag{9}$$

Alternatively, when quadratic interpolation is applied, the scheme (Q-Bouzidi) has the following form for $q < 0.5$:

$$f_{\bar{\alpha}}(\boldsymbol{r}_f, t + \Delta t) = q(1 + 2q)\tilde{f}_\alpha(\boldsymbol{r}_f, t) + (1 - 4q^2)\tilde{f}_\alpha(\boldsymbol{r}_{ff}, t) - q(1 - 2q)\tilde{f}_\alpha(\boldsymbol{r}_{fff}, t), \tag{10}$$

and for $q \geqslant 0.5$,

$$f_{\bar{\alpha}}(\boldsymbol{r}_f, t + \Delta t) = \frac{1}{q(2q + 1)}\tilde{f}_i(\boldsymbol{r}_f, t) + \frac{2q - 1}{q}\tilde{f}_{\bar{\alpha}}(\boldsymbol{r}_f, t) - \frac{2q - 1}{2q + 1}\tilde{f}_{\bar{\alpha}}(\boldsymbol{r}_{ff}, t). \tag{11}$$

It can observed that in the Bouzidi schemes, the unknown values of distribution functions are solved at the fluid nodes using an interpolation technique.

C. Unified schemes (L-Uni and Q-Uni) [25]

The Bouzidi scheme requires separate treatments for $q < 0.5$ and $q \geqslant 0.5$ that may cause an abrupt change in calculated distribution function when q changes from less than 0.5 to more than 0.5 (as in moving boundaries). To overcome this issue, a unified version of the Bouzidi scheme was proposed by Yu *et al.* [25]. The linear interpolation of Yu scheme (L-Uni) is written as

$$f_{\bar{\alpha}}(\boldsymbol{r}_f, t + \Delta t) = \frac{1}{1 + q}[q\tilde{f}_\alpha(\boldsymbol{r}_f, t) + (1 - q)\tilde{f}_\alpha(\boldsymbol{r}_{ff}, t) + q\tilde{f}_{\bar{\alpha}}(\boldsymbol{r}_f, t)]. \tag{12}$$

If quadratic interpolation is applied [34], the model (Q-Uni) has the form

$$\begin{aligned} f_{\bar{\alpha}}(\boldsymbol{r}_f, t + \Delta t) = \frac{1}{(1 + q)(2 + q)}[&q(1 + q)\tilde{f}_\alpha(\boldsymbol{r}_f, t) \\ &+ 2(1 - q^2)\tilde{f}_\alpha(\boldsymbol{r}_{ff}, t) \\ &- q(1 - q)\tilde{f}_\alpha(\boldsymbol{r}_{fff}, t) + 2q(2 + q)\tilde{f}_{\bar{\alpha}}(\boldsymbol{r}_f, t) \\ &- q(1 + q)\tilde{f}_{\bar{\alpha}}(\boldsymbol{r}_{ff}, t)]. \end{aligned} \tag{13}$$

It can be seen that the Yu scheme does not require conditional branching (by $q <$ or > 0.5). However, compared to the Bouzidi scheme, the Yu scheme involves more operations and distribution function evaluations.

D. Interpolation-free schemes (OSIF and CPIF) [34]

Previous investigations [24] indicated that interpolation-based schemes for treatment of curved boundaries destroy mass conservation at the boundaries. To overcome the drawback of these interpolation-based curved boundary treatments, an interpolation-free technique was proposed by Kao and Yang [34]. The interpolation-free schemes are based on the concept of local grid refinement similar to Filippova and Hänel [40], albeit without the actual grid refinement. The viscosities are

modified depending on the q values, to mimic a finer local grid. In the proposed onsite interpolation-free (OSIF) scheme, the fluid distribution function is computed in the post-collision step and is then streamed to the surface of the solid node $\boldsymbol{r}_b$. For all $0 < q \leqslant 1$,

$$
\begin{aligned}
\tilde{f}_\alpha(\boldsymbol{r}_f,t) = f_\alpha^{\text{eq}}(\boldsymbol{r}_f,t) + [\tilde{f}_\alpha(\boldsymbol{r}_f,t) \\
- f_\alpha^{\text{eq}}(\boldsymbol{r}_f,t)]\frac{q\omega^c(1-\omega^f)}{\omega^f(1-\omega^c)},
\end{aligned}
\tag{14}
$$

where $\omega^c = \omega$, $\omega^f = 2q/(q-1+2\tau)$ and the superscripts c and f denote the coarse- and fine-grid quantities. The composite interpolation-free (CPIF) model, as the name suggests, is a hybrid approach encompassing mid-grid and onsite bounce-back schemes. The viscosity is modified, accordingly resembling a mid-grid bounce back for $q \leqslant 0.5$ and an onsite bounce back for $q > 0.5$. For $q \leqslant 0.5$, the fine-grid relaxation factor is $\omega^f = 4q/(2q-1+2\tau)$ and

$$
\begin{aligned}
\tilde{f}_{\bar{\alpha}}(\boldsymbol{r}_b,t) = f_\alpha^{\text{eq}}(\boldsymbol{r}_f,t) + [\tilde{f}_\alpha(\boldsymbol{r}_f,t) \\
- f_\alpha^{\text{eq}}(\boldsymbol{r}_f,t)]\frac{2q\omega^c(1-\omega^f)}{\omega^f(1-\omega^c)}.
\end{aligned}
\tag{15}
$$

For $q > 0.5$, $\omega^f = 2q/(q-1+2\tau)$ and

$$
\begin{aligned}
\tilde{f}_\alpha(\boldsymbol{r}_f,t) = f_\alpha^{\text{eq}}(\boldsymbol{r}_f,t) + [\tilde{f}_\alpha(\boldsymbol{r}_f,t) \\
- f_\alpha^{\text{eq}}(\boldsymbol{r}_f,t)]\frac{q\omega^c(1-\omega^f)}{\omega^f(1-\omega^c)}.
\end{aligned}
\tag{16}
$$

E. Yin-Zhang scheme [26]

Yin and Zhang [26] proposed a modified version (Yin-Zhang) of the mid-grid BB scheme with moving boundaries [14] based on the velocity at the mid-grid position instead of the boundary velocity. The mid-grid velocity is obtained by interpolating or extrapolating the velocities from the boundary and the fluid node. For this purpose, the midpoint velocity of a boundary lattice link is calculated as follows. With $\Delta = 1 - q$, and for $\Delta \leqslant 0.5$,

$$
\boldsymbol{u}_m = \frac{0.5\boldsymbol{u}(\boldsymbol{r}_b,t) + (0.5-\Delta)\boldsymbol{u}(\boldsymbol{r}_f,t)}{1-\Delta}
\tag{17}
$$

and for $\Delta > 0.5$,

$$
\boldsymbol{u}_m = \frac{1.5\boldsymbol{u}(\boldsymbol{r}_b,t) - (\Delta-0.5)\boldsymbol{u}(\boldsymbol{r}_{ff},t)}{2-\Delta}.
\tag{18}
$$

This midpoint velocity is utilized to calculate the bounced-back distribution functions as

$$
f_{\bar{\alpha}}(\boldsymbol{r}_f,t+\Delta t) = \tilde{f}_\alpha(\boldsymbol{r}_f,t) - \frac{2w_\alpha\rho(\boldsymbol{r}_f,t)}{c_s^2}\boldsymbol{u}_m \cdot \boldsymbol{e}_\alpha.
\tag{19}
$$

It is worth mentioning that from a coding perspective, when using the curved boundary schemes, it is more efficient to compute the unknown distribution functions after the streaming step [24]. Streaming simply corresponds to shift of indices of the spatial nodes. This means that $\tilde{f}_{\bar{\alpha}}(\boldsymbol{r}_b,t) = f_{\bar{\alpha}}(\boldsymbol{r}_f,t+\Delta t)$ or $\tilde{f}_\alpha(\boldsymbol{r}_{ff},t) = f_i(\boldsymbol{r}_f,t+\Delta t)$ and so on. Therefore, the curved boundary schemes can also be rewritten based on the distributions after the streaming. Regarding implementation, all the schemes are straightforward to implement. However, the CPIF scheme is slightly complicated due to its combined
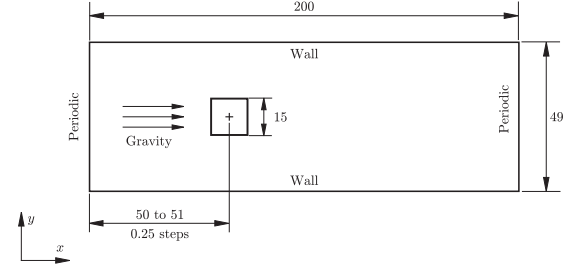

FIG. 2. Simulation setup for flow around a square obstacle, driven by gravity.

mid-grid and onsite bounce-back approach. Regarding computational performance, we observed near similar behavior of all boundary schemes for different test cases and, therefore, the schemes are not compared for execution speed.

IV. RESULTS AND DISCUSSIONS

In this section, the no-slip curved boundary treatments of Sec. III are applied to different flow test cases. Here, the mid-grid bounce-back, linear Bouzidi, quadratic Bouzidi, linear unified, quadratic unified, onsite interpolation-free, composite interpolation-free, and the Yin-Zhang schemes are labeled as MGBB, L-Bouzidi, Q-Bouzidi, L-Uni, Q-Uni, OSIF, CPIF and Yin-Zhang, respectively. Also, we introduce few forced mass conservation cases and a constant density scheme, and investigate their performance.

A. Flow around square cylinder inside a channel

In this test case, we simulate the flow around a square cylinder confined between two parallel walls. The flow is periodic and is driven by gravity. The main advantage of this test case is that all the simulation boundaries are grid aligned. This enables accurate simulation of the flow field using mid-grid bounce-back scheme and subsequently compare different boundary conditions for arbitrary position of the obstacle. The simulated test case is shown in Fig. 2 and is made of 200×51 nodes. The top and bottom walls of the channel are positioned halfway between their respective solid-fluid nodes. Effectively, the channel width is of 49 lattice units. The square obstacle is of size 15×15 lattice units. Different boundary conditions are tested with obstacle at different positions with the centers (C_x) starting from 50 to 51 along x axis in 0.25 increments. All four sides of the obstacle are halfway between the solid-fluid node for the initial and final C_x positions, i.e., $C_x = 50$ and 51. The top and bottom sides of the obstacle are always halfway between solid-fluid nodes for all C_x. In other words, the q values for top and bottom sides of the square are always equal to 0.5, whereas q values change for front and rear sides of the square for different C_x.

Two different Re are simulated by appropriately changing the gravity: one with steady flow at Re = 150 and another with unsteady flow at Re = 330. Here, Re = $U_m H/\nu$ with U_m being the average x-velocity component (U_x) measured at the outflow of the domain and H is the domain height. It should be noted that the viscosity is maintained low such that the Re is high in order to deliberately amplify the mass leakage effects.
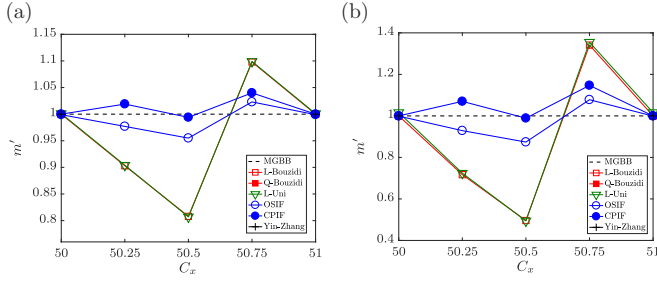
FIG. 3. Change in system mass (m') for different obstacle positions (C_x), for (a) Re = 150 (steady flow) and (b) Re = 330 (unsteady flow). It should be noted that the scales are different for different Re. The data for Q-Bouzidi and Yin-Zhang schemes are available only for $C_x = 50$ and 51.

The relaxation time is maintained at $\tau = 0.52$ for both cases. At the same time, the maximum lattice velocity is kept below 0.15 to avoid compressibility effects.

The metrics we use to analyze the results are the change in system mass (m') at the end of simulations, the normalized flow rate (Q'), and the normalized drag (F_D'). The change in system mass is given by $m' = m_{BC}/m_{initial}$ with mass m being the sum of densities of all fluid nodes, $m = \sum_{i=fluid} \rho_i$. The subscript BC denotes the final condition and "initial" denotes the initial condition of the tested boundary scheme. The simulations are run for 130 000 and 150 000 time steps for Re = 150 and 330, respectively. The normalized flow rate is given by $Q' = Q_{BC}/Q_{MGBB}$ with $Q = \int_0^H U_x\, dy$ at the outlet of the channel. The normalized force is given by $F' = F_{BC}/F_{MGBB}$. Here, the subscripts BC and MGBB denote the tested boundary condition and the mid-grid bounce back, respectively. The m', Q', and F_D' for different schemes are shown in Figs. 3, 4, and 5, respectively. It can be observed that the mass leakage is dependent on the Re on comparing Figs. 3(a) and 3(b) and increases for increasing Re.

The MGBB scheme is perfectly mass conserving and therefore serves as reference in Figs. 3–5. The linear Bouzidi scheme recovers perfectly mass conserving MGBB scheme, if the walls are exactly halfway. The walls are exactly halfway (i.e., $q = 0.5$) on all sides for square obstacle at $C_x = 50$ and 51. In Fig. 3(b), the same can also be observed, i.e., perfectly mass conserving nature of linear Bouzidi scheme. The same was also observed for quadratic Bouzidi scheme, i.e., perfect conservation at $C_x = 50$ and 51. However, the
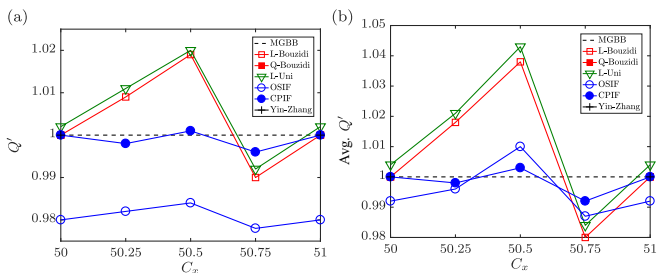

FIG. 4. Normalized flow rate (Q') for different obstacle positions (C_x), for (a) Re = 150 (steady flow) and (b) Re = 330 (unsteady flow).

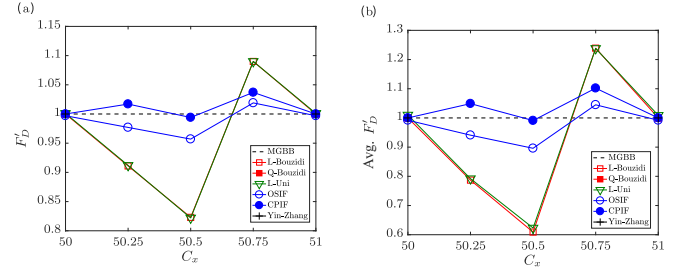FIG. 5. Normalized drag (F_D') for different obstacle positions (C_x), for (a) Re = 150 (steady flow) and (b) Re = 330 (unsteady flow).

quadratic scheme requires much finer grid and higher viscosity (or lower grid Re) for arbitrary wall positions and therefore not stable for C_x other than $C_x = 50$ and 51.

It has to be noted that the linear unified scheme (L-Uni) does not recover MGBB, even for $q = 0.5$ as in the Bouzidi scheme. The same can be verified in Fig. 3(b) that there is a minor mass leakage even at $C_x = 50$ and 51. This is more apparent from the deviation of the normalized flow rate (Q') in Fig. 4(b). The quadratic unified scheme [34] failed for all the test cases. However, the scheme performed stable on a finer grid with higher viscosity to simulate same flow Re.

Also, the Yin-Zhang boundary condition with velocity interpolation or extrapolation was unstable for all positions except for $C_x = 50$ and 51, where it recovers the mid-grid bounce-back condition. The low viscosity, needed to reach high Re at reasonable grid size, exposed the instability of different boundary conditions, especially the quadratic schemes and also the Yin-Zhang boundary condition, which were found only stable for higher relaxation times (for $\tau = 0.6$) and a finer grid. This implies that for high Re flows, the application of such boundaries is limited. More precisely, to simulate a specific flow Re, such schemes require a finer grid with higher τ (or low grid Re) than the other stable schemes.

It could be observed that the OSIF and the CPIF schemes perform better than all other schemes. Overall, CPIF performs best due to its composite design to recover both mid-grid and onsite bounce-back schemes. However, it should be noted that for other intermediate positions, such as $C_x = 50.25$ and 50.75, there is still a mass leakage for CPIF. The highest mass leakage of around 15% is observed at $C_x = 50.75$ for Re = 330 [see Fig. 3(b)]. At $C_x = 50.5$, q becomes zero for the right wall of the square. Therefore, we use $C_x = 50.49$ for OSIF and CPIF as their working range is for $0 < q \leqslant 1$. For the same reason, there is a minor leakage observed for CPIF for both Re at $C_x = 50.5$.

The mass leakage phenomenon would be acceptable provided that the flow field and force experienced by the object are not affected strongly. In reality, both the flow field and the force experienced by the object could be correlated with the mass leakage. Further, if the simulations are run for a longer duration, the mass leakage increasingly affects the simulation results. The linear Bouzidi scheme, which leaks up to 50% at $C_x = 50.5$ [see Fig. 3(b)] shows a corresponding Q' of 4% [see Fig. 4(b)]. Similarly, the corresponding F_D' deviates up to 40%, as can be observed from Fig. 5(b). Even the best performing CPIF scheme shows up to a deviation of 1% for Q' and 10%

deviation for F'_D. Therefore, it can be concluded that none of the available schemes are perfectly mass conserving.

B. Forced mass conservation schemes and constant density scheme

To solve the mass leakage, one can enforce mass conservation by explicitly adding or removing mass from the system. There are several ways to explicitly conserve the mass and at the same time conserve local momentum. The following first four cases conserve both mass and momentum. The last proposed case is slightly different and does not enforce mass conservation. Due to its simplicity, we test these corrections on the popularly used linear Bouzidi scheme. However, it should be observed that these concepts are general and can be applied on any curved boundary scheme.

Case 1: Adding the *local* change in mass per time step ($\delta\rho$), only to the rest distribution of the particular fluid node: $f_0 = f_0 + \delta\rho$.

Case 2: Adding the *local* change in mass per time step, to the distributions of the particular fluid node, multiplied by the corresponding weights: $f_\alpha = f_\alpha + w_\alpha \delta\rho$.

Case 3: Computing the *global* change in mass per time step and evenly adding it to the rest distribution of all fluid nodes: $f_0 = f_0 + \sum \delta\rho/N_f$, where N_f is the total number of fluid nodes.

Case 4: Computing the *global* change in mass per time step and adding it to the distributions proportional to the weights: $f_\alpha = f_\alpha + w_\alpha \sum \delta\rho/N_f$. It should be noted that for cases 2 and 4, the density corrections are applied after the force measurements. Otherwise, the modified distributions would corrupt the actual force experienced by the particle. This implies that an additional variable needs to be introduced to save the leakage amount for individual fluid nodes. Therefore, from an implementation point of view, cases 1 and 3 are simpler to implement.

Case 5: Additionally, we discuss a special case, denoted as case 5, based on the constant density approach [41], where the f_{eq} is given by

$$f_\alpha^{\text{eq}} = w_\alpha \left\{ \rho + \rho_0 \left[\frac{(\boldsymbol{e}_\alpha \cdot \boldsymbol{u})}{c_s^2} + \frac{(\boldsymbol{e}_\alpha \cdot \boldsymbol{u})^2}{2c_s^4} - \frac{(\boldsymbol{u} \cdot \boldsymbol{u})}{2c_s^2} \right] \right\}. \quad (20)$$

Here, ρ_0 is the constant density (equal to the initial density) and the momentum defined as $\rho_0 \boldsymbol{u} = \sum_\alpha f_\alpha \boldsymbol{e}_\alpha$. Further, the forcing term also involves a constant density term $S_\alpha = -3w_\alpha \rho_0 (\boldsymbol{g} \cdot \boldsymbol{e}_\alpha)$ in Eq. (1). It should be noted that ρ_0 is used here instead of ρ earlier. Therefore, the fluid is driven with constant force instead of constant gravity otherwise. As can be seen, this scheme is different from the other four cases because it does not enforce mass conservation. This means that the system mass m, defined as $\sum \rho$, is actually changing with time. However, as the essential parts of the scheme are based on the constant density ρ_0 instead of the actual density $\rho = \sum_\alpha f_\alpha$, the flow field and the forces experienced by the particle are not influenced by the mass leakage.

All the four strict mass conservation schemes are originally conceived by us. However, we later found some literatures have applied such corrections, albeit only in a specific form, only case 1, i.e., adding the local mass leakage to the rest node [42]. Only in this paper, we study different combinations of mass
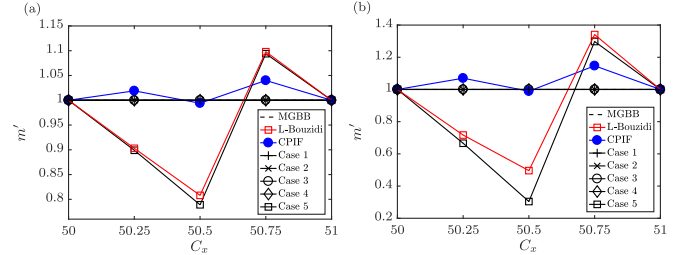

FIG. 6. Change in system mass (m') for different obstacle positions (C_x), for (a) Re = 150 (steady flow) and (b) Re = 330 (unsteady flow).

correction and their effects on flow field in a detailed manner and thereby make useful suggestions to the LBM community.

Each of the above mentioned cases is unique and will have its own implication to the flow field. Next, we apply these cases to the previous test case and observe their performance. The performances are compared with the linear Bouzidi scheme without correction and also with the best performing CPIF scheme. The m' for different cases are given in Fig. 6. Due to their perfectly conserving nature, there is no deviation in system mass m' for cases 1–4, as can be seen from both Figs. 6(a) and 6(b). Case 5 shows slightly higher mass leakage than the original linear Bouzidi scheme as it is not a mass conservation enforcing scheme.

The Q' for the different cases are given in Fig. 7. In terms of flow fields, we observe that both cases 1 and 2 have similar performance, both performing better than the CPIF scheme for the steady flow, as can be seen in Fig. 7(a). For unsteady flows, again a similar performance from cases 1 and 2 with a comparable performance of CPIF, but slightly poorer only at $C_x = 50.5$. This is because the Bouzidi scheme does not recover onsite bounce back, which occurs for $C_x = 50.5$ for the front and rear sides of the obstacle. The cases 3–5 perform almost similar with slightly higher deviations shown by case 5. Importantly, it should be noted that all cases perform better than the original Bouzidi scheme. Therefore, we recommend the use of any explicit mass conserving scheme, specifically cases 1 and 2, which offer superior performance among the investigated cases.

For F'_D, it can be observed that all cases perform identical and show far superior performance over the CPIF scheme itself, as seen in Figs. 8(a) and 8(b). Similarly from Q', we conclude that the explicit mass conservation as in cases 1–4
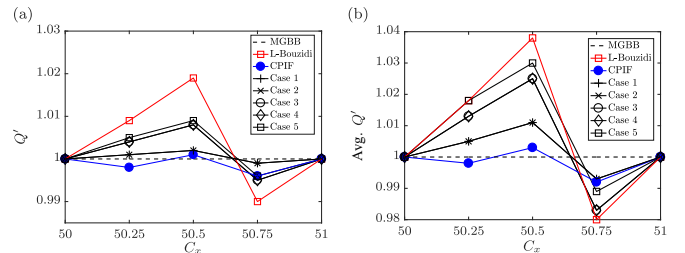

FIG. 7. Normalized flow rate (Q') for different obstacle positions (C_x), for (a) Re = 150 (steady flow) and (b) Re = 330 (unsteady flow).
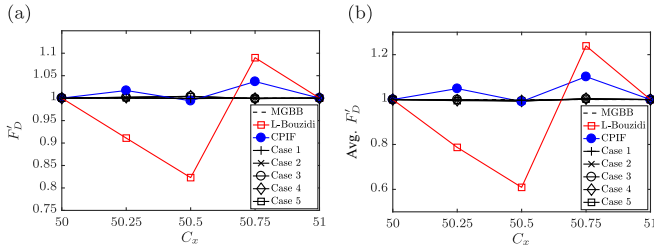
FIG. 8. Normalized drag (F'_D) for different obstacle positions (C_x), for (a) Re = 150 (steady flow) and (b) Re = 330 (unsteady flow).

FIG. 10. The normalized system mass (m') of different schemes for the inclined channel flow over time.

and constant density approach of case 5 provide better accuracy than the existing schemes without explicit mass conservation. Even though case 5 shows significant mass leakage, the case performs better in terms of computing the true velocity field as observed from Q' and also in terms of force experienced by the obstacle as in F'_D compared to conventional linear Bouzidi scheme.

Next, we analyze the flow field in detail for steady flow occurring at Re = 150. The horizontal velocity component (U_x) is measured along the centerline of the domain. Here, we consider the worst performing condition of the linear Bouzidi scheme, which occurs at $C_x = 50.5$. Then, we apply the proposed methods and compare their performance. The U_x for the different cases are plotted in Fig. 9. The results are compared with the true solution obtained from the mid-grid bounce-back (MGBB) scheme. To maintain consistency, the MGBB results are shifted by 0.5 along the x direction. From the results, it can be observed that there is a large deviation of the linear Bouzidi solution from the MGBB solution. However, on applying the methods proposed, it is observed that the resulting flow field is closer to the true solution (of the MGBB). As mentioned earlier, cases 1 and 2 perform identical and are closest to the solution obtained from MGBB, which is evident from the zoomed Figs. 9(b)–9(d). Likewise, cases 3, 4, and 5 perform identical and are slightly away from the MGBB
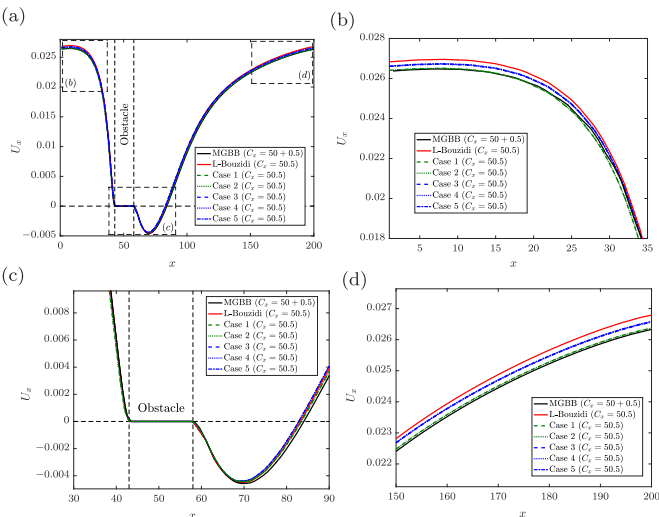
solution, but still better than the linear Bouzidi solution without any correction.

The characteristic of the current test case is that the walls are flat and are perfectly aligned to the grid. This implies, for a particular wall, the interpolation distances q_α are the same for all wall-intersecting directions. Further, the test case replicates flow conditions with strong pressure gradients, and therefore strong density gradients, in the stagnation flow in front of the square object.

C. Flow through an inclined channel

In this section, we simulate a pure shear flow through a periodic channel driven by gravity. To include effects of different interpolation distances q_α, we simulate the flow in an inclined channel. With this simulation, we investigate the effects of mass leakage on pure shear flows. The channel width is 7 lattice units and the channel has an inclination of 3/5. The simulation parameters are $\tau = 0.52$ and $g = 10^{-4}$. The change in system mass after 20 000 time steps for different schemes is plotted in Fig. 10 and the resulting flow profile for different schemes is plotted in Fig. 11. The flow velocities are normalized against the maximum velocity obtained from the theory.

Regarding the performance of different schemes, the quadratic schemes perform better than linear schemes, even though τ is low. The results are not shown here for brevity and the interested reader can refer to Fig. 2 of Bouzidi *et al.* [22]. Therefore, it can be inferred that the quadratic schemes
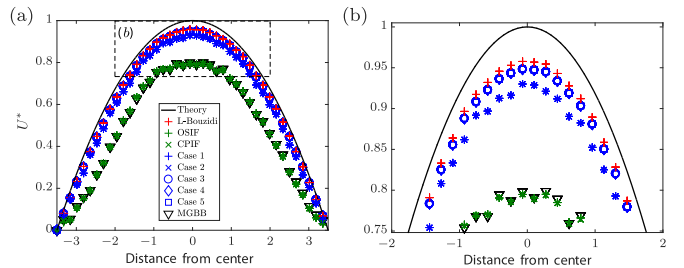

FIG. 9. Distribution of horizontal velocity component U_x for different schemes.

FIG. 11. The normalized tangential velocity (U^*) of the flow inside a straight channel with an inclination of 3/5. (b) Zoom-in of the full velocity profile shown in (a).

are stable, even with low τ, for flows with no density gradient, as in the pure shear flow in this test case. However, due to poor stability in flows with density gradients, as seen from previous test case, these schemes are not considered for further comparison.

The different schemes achieve steady velocity profiles even after the steady leaking of the mass. Among the schemes shown, the linear Bouzidi scheme showed best performance. The performances of both the OSIF and CPIF schemes are poor and are comparable to that of the staircase approximation of the mid-grid scheme. The reason why the interpolation-free schemes perform poor could be due to different q_α values for a boundary fluid node for different directions. In the previous test case, the q_α values are identical for all intersecting velocity directions for a particular side. The interpolation-free schemes are based on varying the viscosity depending on the q_α. Therefore, having different q_α for different velocity directions within a fluid node implies using different viscosities for a single fluid node. These simultaneous effects can affect the performance of the schemes.

Among the five cases proposed, cases 1 and 2 performed slightly poorer than other correction cases. The reason why such cases perform poorly is due to the fact the mass corrections are applied locally at the boundary. The complete or significant part of the correction goes to the rest distribution f_0 and therefore could slightly increase the pressure locally, resulting in slight pressure fluctuations on the boundary. The cases 3, 4, and 5 perform identical and only slightly poorer than the linear Bouzidi scheme. This is contrary to the previous test case, where all the cases performed better than the default linear Bouzidi scheme. However, it should be noted that many practical LBM simulations involve both shear and pressure effects. Therefore, we next select a test case which involves both shear and stagnation pressure effects.

D. Flow around staggered circular cylinders

In order to emulate a general particulate system or a porous medium, we simulate here periodic flow around staggered circular cylinders. Inline cylinders are avoided as it would result in flow channeling at higher Re and thereby purely dominated by shear effects alone. The staggered configuration considered here provides a good mix of stagnation and shear effects. The flow setup is shown in Fig. 12. The solids-volume
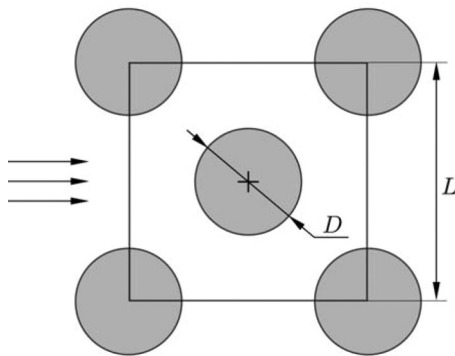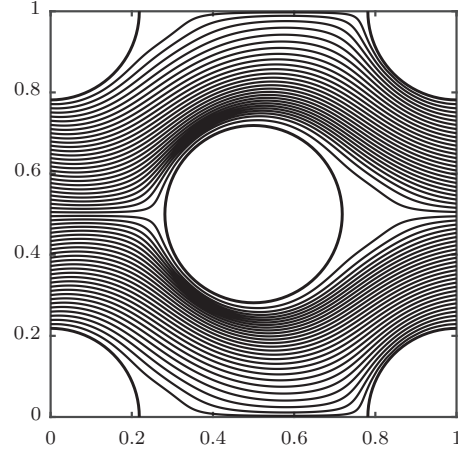

FIG. 13. The accurate velocity field for Re $= 40$ obtained using the mid-grid bounce-back scheme with very high grid resolution.

fraction ϵ_s is 0.3 and the cylinder diameter D is chosen appropriately, depending on the domain size.

Since there is no analytic solution available for such a flow problem, a highly accurate solution is obtained with $D = 131.1$ in a 300×300 domain with the mid-grid bounce-back scheme. The simulation has been performed for Re $= 40$ with Re $= U_0 D / \nu$. The flow is steady for this flow configuration. Here, $U_0 = (1 - \epsilon_s) U_{av}$ is the superficial fluid velocity with U_{av} the average velocity in the fluid domain. Since the flow is driven by gravity and the velocity field evolves accordingly, a feedback loop is used to control the gravity to achieve the desired U_0 precisely. The resulting velocity field is shown in Fig. 13. The drag coefficient is computed as $C_D = F_D / (1/2 \rho D U_0^2)$, where F_D is the drag acting on a single cylinder. A value of $C_D = 5.93$ is obtained for the highly refined grid.

Next, we simulate a domain of size 30×30 with the different boundary conditions, for the same Re, for 20 000 time steps. Based on the accurate C_D computed before, the true drag ($F_{D,\text{true}}$) for the new resolution is computed. We measure the F_D for the different boundary schemes from the simulations and compare with the $F_{D,\text{true}}$ as $F'_D = F_D / F_{D,\text{true}}$. The evolution of mass leakage is plotted in Fig. 14. The

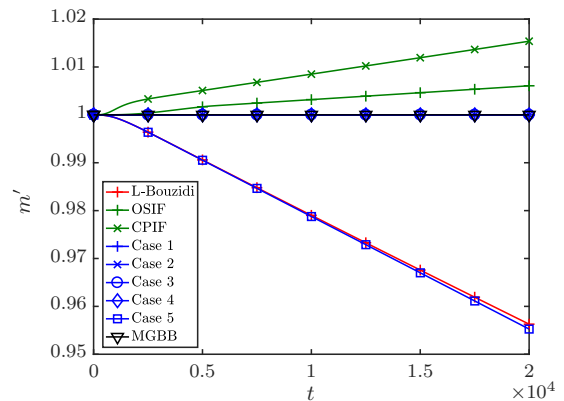FIG. 12. The staggered cylinder configuration: The domain is periodic and the flow is driven by gravity.

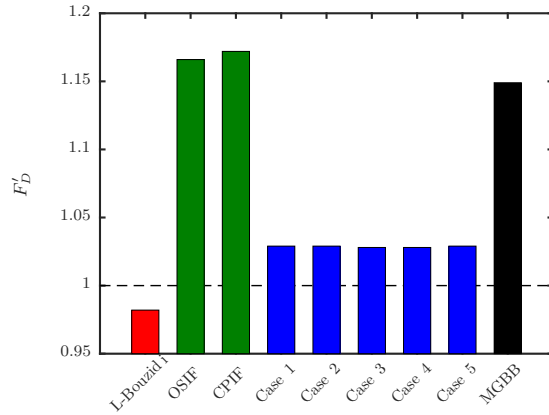FIG. 14. The normalized system mass (m') of different schemes for the periodic flow around staggered cylinders.

FIG. 15. The normalized drag (F_D') of different schemes for the periodic flow around staggered cylinders. It should be noted that F_D' of L-Bouzidi scheme, though it appears closest to 1, is time dependent. This implies a longer simulation would result in F_D' further away from 1. Only the results of cases 1–5 and MGBB are time independent.

normalized drag F_D' is plotted in Fig. 15. It should be noted that the first three schemes in Fig. 15, the Bouzidi and interpolation-free schemes, have drag dependent on the average density of the system. This implies that they are dependent on the simulation duration and exhibit different drag for a longer simulation. In other words, although the linear Bouzidi scheme exhibits F_D' closest to 1, it should be noted that a longer simulation would imply a different F_D' with larger deviation due to mass leakage. For the cases 1–5, the force observed is independent of time, including case 5 which exhibits mass leakage. Further, it can be observed that the proposed correction cases perform better than the mid-grid bounce back, which experiences higher drag on the particle due to the staircase approximation of the geometry. Overall, the cases 3 and 4 performed slightly better ($F_D' = 1.028$) than all other cases ($F_D' = 1.029$).

V. RECOMMENDATIONS FOR PRACTICAL USE

Among the five correction schemes proposed, we observed that cases 1 and 2 (enforcing local mass conservation) performed relatively better for flows with large stagnation effects. However, we also found that their performance is slightly poorer in case of pure shear flows. This could be attributed to the fact that they are local correction schemes, which introduce local pressure differences on the boundaries. On the other hand, global correction schemes such as cases 3 and 4 perform relatively better in case of pure shear flows and also for flow around staggered cylinders. Therefore, global correction schemes (cases 3 and 4) are recommended if mass conservation is a desired property for the system. Furthermore, case 3 is easier to implement than 4. Mass corrections need

to be performed after the force measurement for case 4 as the nonrest distributions are modified for case 4. Therefore, we can conclude that case 3, globally correcting the mass by distributing the correction over all fluid node rest distributions, would be the best choice among the different correction schemes proposed.

VI. CONCLUSION

We tested different curved no-slip boundary conditions for LBM available in the literature with a focus on mass leakage at high Re. Several test cases were proposed, such as periodic flow around a square cylinder, periodic inclined channel flow, and periodic flow around staggered cylinders. The performance of different schemes was tested based on the mass leakage, flow velocity, and the resulting force exerted by the fluid flow. The results were also compared to analytical solutions, where available.

Generally for flows exhibiting strong pressure gradients, we observed that quadratic schemes are unstable at low viscosities. However, for pure shear flows, they are relatively stable and achieve better performance compared to linear schemes. Overall, the linear schemes performed better in terms of stability. We also observed that the variable viscosity interpolation-free schemes such as the OSIF and CPIF were stable for different flows. However, their performance was poor in terms of accuracy for curved boundaries or boundaries with different q_α as in inclined channel flow. The Yin-Zhang scheme has been found to be unstable for flows with high pressure gradients and is therefore not recommended on the basis of stability. For stable cases, the Yin-Zhang scheme did not yield better performance than the linear Bouzidi scheme.

Apart from different existing boundary conditions, we have also tested four different cases where mass conservation was explicitly enforced and one constant density case, applied on the linear Bouzidi scheme. For flows with large stagnation effects, we observed that enforcing local mass conservation performed slightly better than global correction schemes. However, for pure shear flows, the global correction schemes performed much better than local schemes. In a general flow problem with combined shear and stagnation effects, we observe that global correction schemes perform better than local correction schemes. Overall, we recommend case 3 type correction (global correction of the fluid node rest distributions) considering the ease of implementation.

[1] C. K. Aidun and J. R. Clausen, Annu. Rev. Fluid Mech. **42**, 439 (2010).

[2] M. C. Sukop and D. T. Thorne, *Lattice Boltzmann Modeling: An Introduction for Geoscientists and Engineers* (Springer, Berlin, 2006).

[3] A. Zarghami, N. Looije, and H. Van den Akker, Phys. Rev. E **92**, 023307 (2015).

[4] N. A. C. Sidik and R. Mamat, Int. Commun. Heat Mass Transfer **66**, 11 (2015).

[5] A. Zarghami, G. Falcucci, E. Jannelli, S. Succi, M. Porfiri, and S. Ubertini, Int. J. Mod. Phys. C **25**, 1441012 (2014).

[6] S. Succi, *The Lattice Boltzmann Equation: For Fluid Dynamics and Beyond* (Oxford University Press, Oxford, 2001).

[7] D. A. Wolf-Gladrow, *Lattice-Gas Cellular Automata and Lattice Boltzmann Models: An Introduction* (Springer, Berlin, 2004).

[8] D. P. Ziegler, J. Stat. Phys. **71**, 1171 (1993).

[9] D. R. Noble, S. Chen, J. G. Georgiadis, and R. O. Buckius, Phys. Fluids **7**, 203 (1995).

[10] T. Inamuro, M. Yoshino, and F. Ogino, Phys. Fluids **7**, 2928 (1995).

[11] P. A. Skordos, Phys. Rev. E **48**, 4823 (1993).

[12] J. Latt, B. Chopard, O. Malaspinas, M. Deville, and A. Michler, Phys. Rev. E **77**, 056703 (2008).

[13] S. Chen, D. Martinez, and R. Mei, Phys. Fluids **8**, 2527 (1996).

[14] A. J. C. Ladd, J. Fluid Mech. **271**, 311 (1994).

[15] A. J. C. Ladd and R. Verberg, J. Stat. Phys. **104**, 1191 (2001).

[16] D. Kandhai, A. Koponen, A. Hoekstra, M. Kataja, J. Timonen, and P. M. A. Sloot, J. Comput. Phys. **150**, 482 (1999).

[17] O. Filippova and D. Hänel, Comput. Fluids **26**, 697 (1997).

[18] R. Mei, L.-S. Luo, and W. Shyy, J. Comput. Phys. **155**, 307 (1999).

[19] Z. Guo, C. Zheng, and B. Shi, Phys. Fluids **14**, 2007 (2002).

[20] J. Kang, S. Kang, and Y. K. Suh, J. Mech. Sci. Technol. **22**, 1192 (2008).

[21] A. Tiwari and S. P. Vanka, Int. J. Numer. Methods Fluids **69**, 481 (2012).

[22] M. Bouzidi, M. Firdaouss, and P. Lallemand, Phys. Fluids **13**, 3452 (2001).

[23] I. Ginzburg and D. d'Humières, Phys. Rev. E **68**, 066614 (2003).

[24] P. Lallemand and L.-S. Luo, J. Comput. Phys. **184**, 406 (2003).

[25] D. Yu, R. Mei, and W. Shyy, A unified boundary treatment in lattice Boltzmann method, in *41st Aerospace Sciences Meeting and Exhibit, Aerospace Sciences Meetings*, AIAA Paper No. 2003-953 (AIAA, 2003).

[26] X. Yin and J. Zhang, J. Comput. Phys. **231**, 4295 (2012).

[27] Z.-G. Feng and E. E. Michaelides, J. Comput. Phys. **195**, 602 (2004).

[28] K. Suzuki and T. Inamuro, Comput. Fluids **49**, 173 (2011).

[29] I. Ginzburg, F. Verhaeghe, and D. d'Humières, Commun. Comput. Phys. **3**, 519 (2008).

[30] O. R. Mohammadipoor, H. Niazmand, and S. A. Mirbozorgi, Phys. Rev. E **89**, 013309 (2014).

[31] R. W. Nash, H. B. Carver, M. O. Bernabeu, J. Hetherington, D. Groen, T. Krüger, and P. V. Coveney, Phys. Rev. E **89**, 023303 (2014).

[32] H. Chen, C. Teixeira, and K. Molvig, Int. J. Mod. Phys. C **9**, 1281 (1998).

[33] M. Rohde, J. J. Derksen, and H. E. A. Van den Akker, Phys. Rev. E **65**, 056701 (2002).

[34] P.-H. Kao and R.-J. Yang, J. Comput. Phys. **227**, 5671 (2008).

[35] J. Bao, P. Yuan, and L. Schaefer, J. Comput. Phys. **227**, 8472 (2008).

[36] E. Le Coupanec and J. C. G. Verschaeve, Math. Comput. Simul. **81**, 2632 (2011).

[37] S. K. P. Sanjeevi and J. T. Padding, J. Fluid Mech. **820**, R1 (2017).

[38] L.-S. Luo, Lattice-gas automata and lattice Boltzmann equations for two-dimensional hydrodynamics, Ph.D. thesis, Georgia Institute of Technology, 1993.

[39] D. Yu, R. Mei, L.-S. Luo, and W. Shyy, Prog. Aerospace Sci. **39**, 329 (2003).

[40] O. Filippova and D. Hänel, J. Comput. Phys. **147**, 219 (1998).

[41] X. He and L.-S. Luo, J. Stat. Phys. **88**, 927 (1997).

[42] X. Yin, G. Le, and J. Zhang, Phys. Rev. E **86**, 026701 (2012).